The Astrophysical Journal, 722:273–280, 2010 October 10 doi:10.1088/0004-637X/722/1/273

DETECTION OF MULTIPLE BIPOLAR FLOWS IN NGC 7027 WITH SUBMILLIMETER ARRAY

Zhen-Yuan Huang[1,2], Tatsuhiko I. Hasegawa[1], Dinh-V-Trung[1,3], Sun Kwok[1,4], Sebastien Muller[1,5], Naomi Hirano[1], Jeremy Lim[1,4], C. Muthu Mariappan[1,6], and Aran Lyo[1,7]
[1] Institute of Astronomy and Astrophysics, Academia Sinica, P.O. Box 23-141, Taipei 10617, Taiwan; hasegawa@asiaa.sinica.edu.tw, hirano@asiaa.sinica.edu.tw
[2] National Taiwan University, Taipei 10617, Taiwan; astrotrumon@gmail.com
[3] Institute of Physics, Vietnam Academy of Science and Technology, Hanoi, Vietnam; trung@asiaa.sinica.edu.tw
[4] University of Hong Kong, Pokfulam, Hong Kong; sunkwok@hku.hk, jlim@asiaa.sinica.edu.tw
[5] Onsala Space Observatory, Gothenburg, Sweden; sebastien.muller@chalmers.se
[6] Aryabhatta Research Institute, Nainital, Uttaranchal, India; muthu@aries.ernet.in
[7] Korea Astronomy and Space Science Institute, Republic of Korea; arl@kasi.re.kr
Received 2009 December 30; accepted 2010 August 11; published 2010 September 17

ABSTRACT

Highly collimated multiple bipolar flows are detected with a 3″ resolution in the HCO^+ ($J = 3$–2) and HCN ($J = 3$–2) lines in the young planetary nebula NGC 7027 with the Submillimeter Array. The HCO^+ and HCN flows coincide in location and velocity with compact and fast CO flows detected with ∼6″ resolutions with other millimeter arrays. The equatorial molecular torus of NGC 7027 is captured in HCO^+ emission in the present observations. The HCO^+ emission also closely follows the H_2 emission, indicating that the present observations probe the photon-dominated region of the molecular envelope of NGC 7027.

Key words: ISM: molecules – planetary nebulae: individual (NGC 7027)

1. INTRODUCTION

The apparent morphologies of many planetary nebulae (PNe) are approximately explained by an equatorial torus and two bipolar lobes (Balick 1996; Bryce et al. 1994; Zhang & Kwok 1998). A number of PNe, however, have been identified as having multiple pairs of bipolar lobes or multiple outflow axes (Sahai 2000; López et al. 1995). Nevertheless, those so-called multipolar or point-symmetric PNe (and counterparts of protoplanetary nebulae (PPNe)) still retain certain degrees of axial symmetry with rather ubiquitous equatorial tori. Those multiple bilobes do not seem oriented in a random direction with respect to those tori.

The young PN NGC 7027 shows a high degree of axial symmetry with an equatorial torus in early optical images with the *Hubble Space Telescope* (*HST*). Recent observations in the IR and radio, with dramatically improved angular and velocity resolutions, increasingly suggest that NGC 7027 is a multipolar PN in the making while retaining its overall axial symmetry (see below for more details).

The images of the central H II region of NGC 7027 in various wavebands consistently show an elliptical morphology (Masson 1986; Latter et al. 2000; Cox et al. 2002) with a major axis (a full length of 14″) in the northwest to southeast (NW–SE) direction with a position angle (P.A.) of −30°. The central H II region is a prolate spheroidal shell with a density enhancement in the equatorial region (a torus or ring; Cox et al. 2002; Latter et al. 2000; Roelfsema et al. 1991; Atherton et al. 1979). The symmetry axis of the prolate spheroid appears as the projected major axis of the ellipse in the NW–SE direction. The NW part of the three-dimensional symmetry axis is tilted toward the observer from the plane of sky by 45°–55° (Cox et al. 2002; Latter et al. 2000; Roelfsema et al. 1991; Atherton et al. 1979).

The central H II region is surrounded by an approximately spherical CO envelope that extends to 60″ from the center (Jaminet et al. 1991; Phillips et al. 1991; Fong et al. 2006). There appears to be a molecular equatorial torus adjacent to the ionized equatorial torus. The ionized and molecular tori most likely form a single torus structure, where the inner part of the torus has been ionized and the outer part is still in the molecular form (Bieging et al. 1991; Fong et al. 2006). The interface layer between the ionized and molecular regions of NGC 7027 has been captured in H_2 1–0 $S(1)$ by Latter et al. (2000) and Cox et al. (2002). The interface layer has a morphology of an hourglass with a wide waist (Cox et al. 2002; Latter et al. 2000), where the waist part corresponds to the equatorial torus.

The presence of a bipolar outflow in NGC 7027 was suggested in early studies (Phillips et al. 1991; Jaminet et al. 1991; Masson et al. 1985). Likely high-velocity components in molecular gas in NGC 7027 have been detected in CO observations by Masson et al. (1985), Bieging et al. (1991), and Graham et al. (1993). However, it was difficult to separate (geometrically and kinematically) the bilobal hourglass structure, the equatorial structure, and the possible outflow. High-velocity components were also captured in HCO^+ (1–0) by Deguchi et al. (1992) and Likkel (1992). Hasegawa & Kwok (2001) in single dish observations suggested the presences of high-velocity components in CN and HCN as well as HCO^+ associated with the high-velocity components detected in CO. Recently, Fong et al. (2006) successfully isolated, with an angular resolution of 6″, the high-velocity components in CO (1–0) that are oriented in the north–south direction.

There is a puzzling aspect in the possibly bipolar fast components detected in CO and HCO^+. The fast CO flow seems oriented in the north to south (N–S) direction with P.A. = 0° (Fong et al. 2006), whereas the prolate spheroid of the nebula and the hourglass morphology of the photon-dominated region (PDR) have a common symmetry axis in the NW–SE direction (with P.A. = −30° to −40°). If the overall bipolar geometry and the CO outflow have a causal relation (or have a common underlying mechanism), then the two axes would be aligned. The misalignment of the two symmetry axes became undeniable when the IR nebular line and H_2 line observations revealed the structures with a 1″ resolution. Recent CO (1–0) observations by Fong et al. (2006) underscore this puzzle.

Through H_2 line imaging, Latter et al. (2000) and Cox et al. (2002) identified a few pairs of extruding (or bored) structures in the mostly enclosing, smoothly curved layer of the PDR of NGC 7027, where a pair of such structures in point symmetry were identified as a bipolar outflow. Latter et al. (2000) identified two outflows: one with P.A. $= -50^\circ$ (hereafter the L-1 flow) and the other with P.A. $= -30^\circ$ (hereafter the L-2 flow). Cox et al. (2002) identified three outflows: one with P.A. $= -53^\circ$ (hereafter the C-1 flow), the second with P.A. $= +4^\circ$ (hereafter the C-2 flow), and the third with P.A. $= -28^\circ$ (hereafter the C-3 flow). The numbering conventions are taken from the respective papers. Closer inspections of the H_2 images (Latter et al. 2000; Cox et al. 2002) show the L-1 and C-1 flows are identical. Likewise the L-2 and C-3 flows are identical as the similar values in P.A. suggest. Although the P.A. for the C-3 (= L-2) flow is very close to that of the overall symmetry axis of the hourglass structure, the C-3 (= L-2) flow has been identified by Latter et al. (2000) and Cox et al. (2002) from faint and narrow extruding structures. These are possible manifestations of multiple outflows that are very collimated and energetic. The likely multiple collimated outflows could be another examples of the bipolar, rotating, episodic jets (BRETs; Latter et al. 2000).

The peculiar morphological features for identifications of outflows have small (a few arcseconds) sizes (Latter et al. 2000; Cox et al. 2002). These identifications were not easily confirmed on kinematical basis through molecular line observations.

We have observed the HCO^+ and HCN line emissions in NGC 7027 with the Submillimeter Array (SMA). Our observations allow us to identify fast multiple outflows in the emissions of these heavy molecules with an angular resolution much improved from the past CO and HCO^+ imaging observations.

2. OBSERVATIONS

We observed the $J = 3$–2 rotational transitions of HCO^+ (267.5576 GHz) and HCN (265.8864 GHz) in NGC 7027 with the SMA[8] on 2005 July 12 and 15. Six antennas were used in the compact configuration (Ho et al. 2004). The field of view was 48″ at 267 GHz. The projected shortest and longest baselines were 8 m and 69 m, respectively. The synthesized beam was 3.″77 × 2.″38 (P.A. = 119°) with uniform weighting. The emission structures larger than 29″ were likely resolved out. The correlator had an instantaneous frequency coverage of 2 GHz, and the HCO^+ and HCN lines were received simultaneously in the lower sideband with a frequency resolution of 0.812 MHz. The upper (mirror) sideband signal was separately recorded. In order to improve the signal-to-noise ratio (S/N), three channels were binned to one, resulting in a channel width of 2.436 MHz. The resulting velocity resolution is 2.73 km s^{-1} at 267.5576 GHz and 2.75 km s^{-1} at 265.8864 GHz. The continuum emission was measured from line-free channels over a total frequency range of 1872 MHz centered at 266.76 GHz in the lower sideband.

The bandpass calibrations were made with 3C 279 and Uranus in the first and second tracks, respectively. Uranus (with an adopted flux of 67 Jy) was used for flux calibration in the second track and the solution was also applied to the first short one for its lack of planet observations during the observing run. The phase and amplitude were calibrated with QSO B2200+420. The calibrator B2200+420 is a good phase reference owing to its unresolved point structure on the cleaned map. All the calibration results were applied to the NGC 7027 data. We used MIR package, which is IDL-based, for standard calibrations. The calibrated uv data were converted to molecular line and continuum images with the NRAO AIPS package.

[8] The Submillimeter Array (SMA) is a joint project between the Smithsonian Astrophysical Observatory and the Academia Sinica Institute of Astronomy and Astrophysics, and is funded by the Smithsonian Institute and the Academia Sinica.

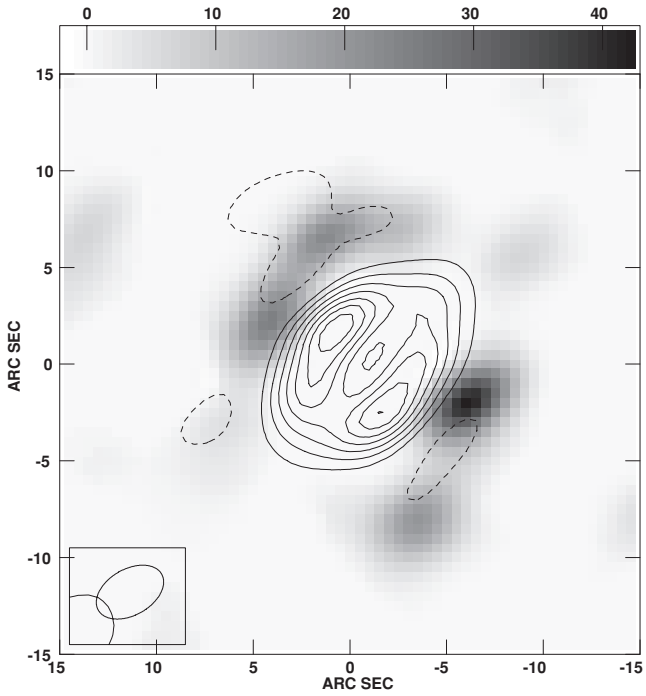

Figure 1. Line-free continuum (contours) at 266 GHz and integrated intensity of HCO^+ (3–2) (gray scale) in NGC 7027. The contours for continuum start at 62 mJy beam^{-1} (3σ) and increase in steps of 3σ. The dashed contours indicate negative values (-3σ). The HCO^+ intensity has been integrated over V_{LSR} = 15.5–34.6 km s^{-1} (systemic velocity ±9.5 km s^{-1}), and the scale (in Jy km s^{-1} beam^{-1}) is shown at the top of the panel. The angular resolution is 3.″77 × 2.″38 with uniform weighting (indicated at the lower left corner of the figure). The map center is R.A.(2000) = 21^{h}07^{m}01.^{s}749, decl.(2000) = 42°14′09.″778.

3. RESULTS

3.1. Continuum

Figure 1 shows the continuum emission and the HCO^+ (3–2) line emission integrated over a velocity width of 19 km s^{-1} centered at $V_{LSR} = 25$ km s^{-1}, the adopted systemic velocity for NGC 7027 in the present work. The continuum emission in the present observation shows an elliptical distribution elongated in the NW–SE direction (P.A. = 135°). The overall size of the continuum emission is 13.″5 × 8.″7 (3σ level). If we adopt a distance of 880 pc (Masson 1989), the size corresponds to (1.78×10^{17}) cm × (1.15×10^{17}) cm. Two emission peaks are found 2.″5 to the northeast (NE) and 2.″8 to the southwest (SW) from the center. The result is very consistent in size and morphology with the past continuum observations (of optically thin free–free emission) in the 2–6 cm bands (Masson 1986; Basart & Daub 1987; Bains et al. 2003) of the central H II region.

The flux density of the continuum in the present measurement is 2.57 Jy for the area above the 3σ (62 mJy per beam) level. This value is about 70% of the continuum fluxes obtained by Hoare et al. (1992, 3.61 Jy) and Knapp et al. (1993, 3.74 Jy) both at 275 GHz (1.1 mm) with an 18″ beam with the James Clerk Maxwell Telescope (JCMT). Figure 13 in Knapp et al. (1993) suggests that the thermal dust emission accounts for about 30% (1.12 Jy) of the flux into the JCMT beam (18″) at 1.1 mm. The dust emission extends beyond the 18″ beam into the molecular

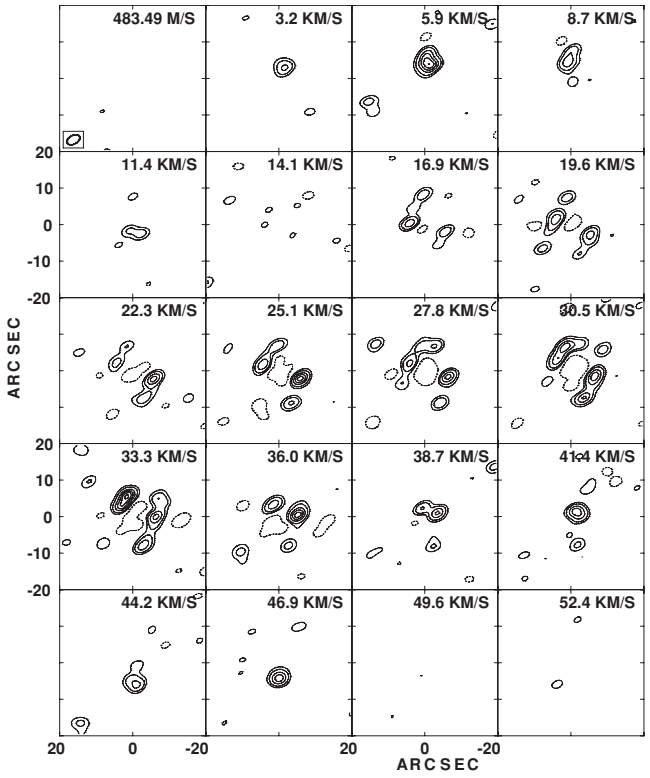

Figure 2. Channel maps of HCO^+ (3–2). The maps have been continuum-subtracted. The channel center velocity (V_{LSR} in km s^{-1}) is indicated at the upper right corner of each panel. Contour levels are 5, 10, 20, 30, 40, and 50 in units of 1.0 Jy $beam^{-1}$ (= 1σ). Dashed contours indicate a negative value (−5σ). The synthesized beam is 3.″82 × 2.″37 (P.A. = 119°) and is shown in the top left panel. The map center is R.A.(2000.0) = $21^h07^m01^s.749$, decl.(2000.0) = 42°14′09.″778.

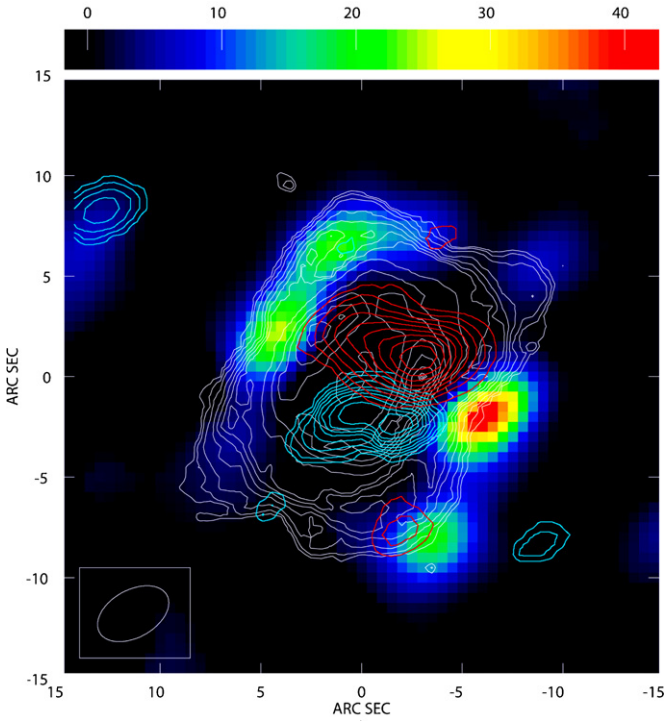

Figure 3. Comparison of HCO^+ (3–2) and H_2 emissions. The white contours represent H_2 emission at 2.12 μm (Latter et al. 2000). The false-color image represents the integrated intensity of HCO^+ emission near the systemic velocity (V_{LSR} = 15.9–34.2 km s^{-1}). The color scale (in Jy km s^{-1} $beam^{-1}$) is given at the top of the panel. The contours in blue and red represent HCO^+ emissions at the bulk expansion velocities of the molecular envelope. The blue contours show the approaching component with V_{LSR} = 10.5–12.3 km s^{-1}. The red contours show the receding component with V_{LSR} = 36.9–42.3 km s^{-1}. The blue (or red) contours start from 10% of the peak intensity of the blue (or red) component, and increase in step of 10%. The blue and red contours correspond to the near and far sides of the equatorial torus, respectively, in the molecular envelope. At the systemic velocity, the prominent emissions of HCO^+ occur in the H_2 emitting region that is considered a PDR.

envelope (Knapp et al. 1993; Hoare et al. 1992). The extended thermal dust emission near 267 GHz has likely been filtered out in the present SMA observation.

3.2. HCO^+ Emission

The integrated HCO^+ (3–2) emission for V_{LSR} = 15.5–34.6 km s^{-1} in Figure 1 shows a ring-like distribution surrounding the ionized region. The distribution of HCO^+ emission is similar to that of H_2 line emission (see Cox et al. 2002 and Latter et al. 2000; see also figures below). Compared with the JCMT observations by Hasegawa & Kwok (2001), 78% of the total HCO^+ flux is missing in the present observation. The fragmented appearances of the emission distributions in the present observations are a result of a combination of filtering out of extended emission and a limited sensitivity to weak emission. Conversely, the present observations selectively probe small-scale structures with enhanced HCO^+ (3–2) emission.

Figure 2 shows channel maps for HCO^+ (3–2). We overlay in Figure 3 the emission spots taken from the channel maps with the H_2 image (Latter et al. 2000). The redshifted emission (V_{LSR} = 37–41 km s^{-1}; red contours in Figure 3) and the blueshifted emission (V_{LSR} = 10–12 km s^{-1}; blue contours in Figure 3) are elongated in the NE–SW direction. Their locations correspond to the waist part of the hourglass morphology of the H_2 emission. The redshifted and blueshifted HCO^+ emissions correspond to the far and near sides of the expanding equatorial torus.

Near the systemic velocity (the false-color image in Figure 3 for V_{LSR} = 16–34 km s^{-1}), the HCO^+ emission (including the two bright spots corresponding to the rim-brightened torus) closely follows the rim-brightened shell structure of H_2 line emission. The present observations do not capture the HCO^+ emission from the near or far side of the expanding, hourglass-shaped wall of the H_2 emission. The CO (1–0) maps by Graham et al. (1993) and the HCO^+ (1–0) maps by Likkel (1992) both show relatively extended (∼20″) emissions around V_{LSR} = 11 km s^{-1} and 39 km s^{-1}. The extended emissions in these CO (1–0) and HCO^+ (1–0) channel maps (Graham et al. 1993; Likkel 1992) likely correspond to the near and far sides of the hourglass-shaped wall that is radially expanding at about 15 km s^{-1}.

Figure 4 shows position–velocity (PV) maps along the major and minor axes of the HCO^+ (3–2) emission. The major axis is taken at a P.A. of −30°. It is roughly the same as the major axes for the H_2 and ionized regions (Cox et al. 2002). The cutting lines (parallel to the minor axis) for Figures 4(a), (b), and (c) are offset by +1.″5, 0″, and −1.″5, respectively, from the minor axis toward the NW direction. (Figure 4(b) represents the cut along the minor axis.)

Three cuts parallel to the minor axis show the encircling pattern of the expanding equatorial torus in the PV phase-space. The torus seen in HCO^+ emission is geometrically thin in the axial and radial directions, resembling the H_2 image. The torus is tilted in such a way that the near side of the torus is seen (in the plane of sky) 2″ SE of the central star. The cut along a line that is

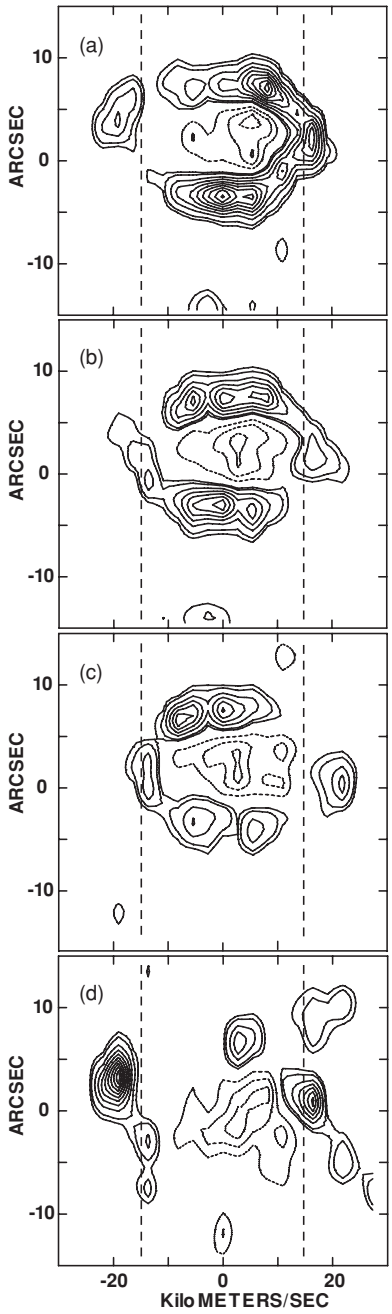

Figure 4. PV maps of HCO^+ (3–2) in NGC 7027. Panels (a), (b), and (c) are cuts parallel to the minor axis (P.A. = 60°) with offsets of 1.″5, 0″, and −1.″5, respectively, from the central star toward NW. Panel (d) is a cut along the major axis (P.A. = 150°) through the central star. The reference position for these maps is the central star and the velocities are relative to V_{LSR} = 25.1 km s^{-1}. The position offsets (*y*-axis) increase toward NE in (a), (b), and (c). The position offsets (*y*-axis) increase toward NW in (d). The thick contours are at 3, 5, 10, 15, 20, 25, 30, 35, 40, 45, 50, and 55 in units of 1σ (=0.1 Jy $beam^{-1}$). The thin contours indicate negative levels at −5, −10, and −15 in units of 1σ.

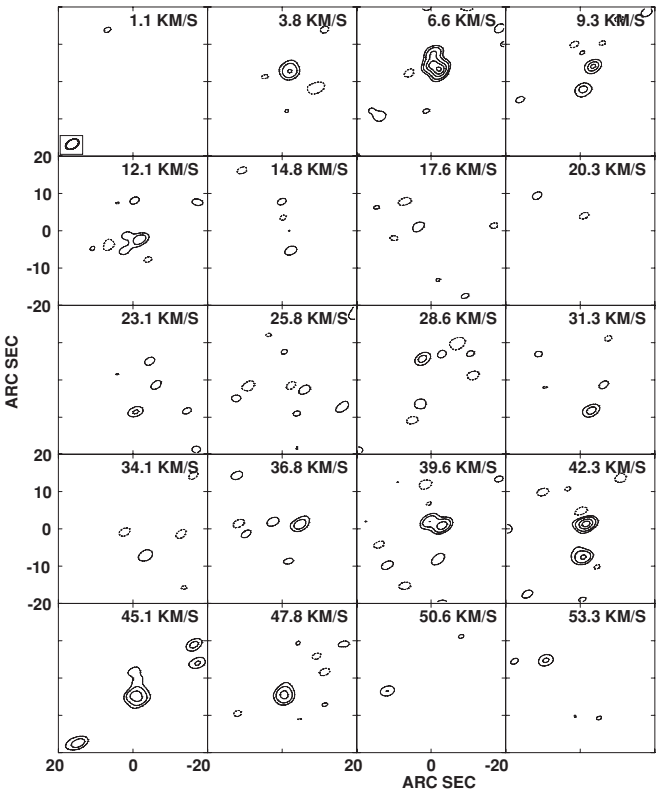

Figure 5. Channel maps of HCN (3–2). The maps have been continuum-subtracted. Contour levels are 5, 10, 20, 30, 40, and 50 in units of 0.74 Jy $beam^{-1}$ (= 1σ). Dotted contours indicate a negative value (−5σ). Otherwise the same as Figure 2.

offset to SE from the center by 1.″5 (Figure 4(c)) shows the near side of the torus, which is blueshifted. The cut along a line that is offset to NW from the center by 1.″5 (Figure 4(a)) shows the far side of the torus, which is redshifted. The most redshifted part in Figure 4(a) reflects the (projected) expansion velocity. The most blueshifted part in Figure 4(c) reflects the (projected) expansion velocity. The detached, blueshifted component in Figure 4(a) is not a part of the torus, as the blueshift exceeds the expansion velocity (indicated by a dashed vertical line) determined from Figure 4(c). The detached, redshifted component in Figure 4(c) is not a part of the torus, as the redshift exceeds the expansion velocity (indicated by a dashed vertical line) determined from Figure 4(a). These fast components have velocity shifts larger than the average expansion velocity of the torus. These fast components are significantly extended to the south and north beyond the geometrical thickness (in the axial direction) of the equatorial torus.

The PV diagram along the major axis shows the cuts of the equatorial ring (at −15 km s^{-1} and +16 km s^{-1}). The dashed lines in Figure 4(d) indicate the expansion velocity of the equatorial ring. Outside the area defined by the dashed lines, we see fast components: (1) strong emission blueshifted more than 15 km s^{-1} with position offsets of about 3″ and (2) weak emission redshifted more than 17 km s^{-1} with position offsets of about −5″.

3.3. HCN Emission

The channel maps for HCN (3–2) are shown in Figure 5. Several bright spots are detected in the present observation. The distribution of the HCN bright spots do not resemble the enclosing molecular envelope seen in CO lines. Compared with the JCMT observations by Hasegawa & Kwok (2001), 80% of HCN flux are missing in the present observation. The total flux of HCN (3–2) is 2.5 times smaller than that of HCO^+ (3–2) in the JCMT observations with a 20″ beam (Hasegawa & Kwok 2001). Most of the HCN (3–2) emission has most likely been either filtered out or below the detection limit in the present observation. Nevertheless, those bright HCN emitting spots can be assigned to the equatorial torus and the outflows, as the locations and velocities of the HCN bright spots coincide well

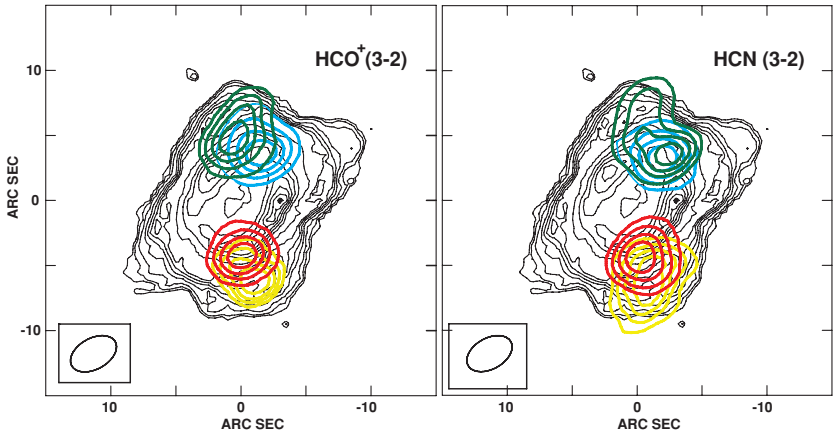

Figure 6. Bipolar outflows of HCO^+ (left) and HCN (right) overlaid on the *HST*/NICMOS H_2 image (black contours; Latter et al. 2000). In both panels, contours in blue indicate the faster approaching components (the H-1 flow in the text), and contours in green indicate the slower approaching components (the H-2 flow in the text). Contours in red indicate the faster receding components (the H-1 flow), and contours in yellow indicate the slower receding components (the H-2 flow). All the colored contours start from 5σ with an increment of 5σ. In the left panel (HCO^+), the velocity range is $V_{LSR} = 1.8$–4.6 km s^{-1} for the blue contours, and is $V_{LSR} = 7.3$–10.1 km s^{-1} for the green contours. For the red contours, $V_{LSR} = 45.5$–48.2 km s^{-1}. For the yellow contours, $V_{LSR} = 42.8$–45.5 km s^{-1}. In the right panel (HCN), the velocity range is $V_{LSR} = 2.4$–5.2 km s^{-1} for the blue contours, and is $V_{LSR} = 5.2$–8.0 km s^{-1} for the green contours. For the red contours, $V_{LSR} = 46.4$–49.2 km s^{-1}. For the yellow contours, $V_{LSR} = 43.7$–46.4 km s^{-1}.

with the HCO^+ emitting spots that correspond to those structures of the molecular regions of NGC 7027.

The near side of the equatorial ring appears in the channel of $V_{LSR} = 9.3$–12.1 km s^{-1} in HCN ($V_{LSR} = 11.4$ km s^{-1} in HCO^+). The far side of the ring appears in the channels of $V_{LSR} = 36.8$–42.3 km s^{-1} in HCN ($V_{LSR} = 36.0$–41.4 km s^{-1} in HCO^+). The near and far sides of the torus correspond to the spike-like features at 10 and 40 km s^{-1} in the single dish spectra. The lowest and highest V_{LSR} values of the near and far sides are 10.5 km s^{-1} and 42.3 km s^{-1}, respectively. The projected expansion velocity of the equatorial torus is 15–16 km s^{-1}. These values for the equatorial torus are consistent with CO observations (Masson et al. 1985; Jaminet et al. 1991; Graham et al. 1993).

3.4. Bipolar Outflows

The fast components mentioned in Section 3.2 appear in the channel maps of HCO^+ (Figure 2) and HCN (Figure 5).

The fast blue components of HCO^+ appear in the channels with $V_{LSR} = 3.2$–8.7 km s^{-1} (blueshifted by 17–23 km s^{-1} from $V_{LSR} = 26$ km s^{-1}; Figure 2). The fast red components of HCO^+ appear in the channels with $V_{LSR} = 44.2$–46.9 km s^{-1} (redshifted by 18–21 km s^{-1} from $V_{LSR} = 26$ km s^{-1}). The fast blue and red HCO^+ components are offset to the north and south, respectively, by 5″. In the early HCO^+ (1–0) observation by Likkel (1992), only the fast blue component is detected. Our HCO^+ (3–2) observations show that there is a fast red counterpart.

The fast blue components of HCN appear in the channels with $V_{LSR} = 3.8$–9.3 km s^{-1} (blueshifted by 17–22 km s^{-1}) in Figure 5. The fast red components of HCN appear in the channels with $V_{LSR} = 45.1$–47.8 km s^{-1} (redshifted by 19–22 km s^{-1}). The fast blue and red HCN components are offset to the north and south, respectively, by 5″.

These fast components in HCO^+ (3–2) and HCN (3–2) are similar, in velocity and location, to high-velocity emission in CO (1–0) observed with the Owens Valley Radio Observatory (Graham et al. 1993). (See the channel maps at $V_{LSR} = 3.5$ and 6.1 km s^{-1} for the fast blue components and at $V_{LSR} = 45.1$ and 47.7 km s^{-1} for the fast red components by Graham et al. 1993.) The high-velocity CO emission is clearly identified by Fong et al. (2006) with Berkeley–Illinois–Maryland Array (BIMA) and its likely geometrical locations are indicated in Figure 13 of Fong et al. (2006).

In the JCMT observations of NGC 7027 in several molecular lines, the wings ($V_{LSR} < 10$ km s^{-1} or $V_{LSR} > 42$ km s^{-1}) of the HCO^+ ($J = 4$–3) and HCN ($J = 4$–3) spectra have been identified as the fast components in contrast to the slow component near the line center (Hasegawa & Kwok 2001). The fast blue and red components are offset to the north and south, respectively, by several arcseconds, although the limited angular resolutions only semi-quantitatively constrained the locations and extents of the fast components. The fast components of HCO^+ (3–2) and HCN (3–2) detected in the present observations have velocities and locations very consistent with the constraints imposed by the single dish observations of the molecules. The fast components in the present observations, therefore, are the fast components detected in the single dish observations.

The locations and extents of the fast components are better constrained in the present work. The fast components are 5″ offset to the north and south. The fast components are compact (a diameter of 5″–7″ for each of the red and blue components) and bright in HCO^+ and HCN as well as in CO. The fast components are regions of enhanced emissions of probably many molecules, as the single dish observations show fast wings in CN and C_2H as well (Hasegawa & Kwok 2001). Overall, the fast components exhibit good point symmetries in velocity and position. These are typical characteristics of a bipolar outflow. The projected direction of the outflow is north–south (P.A. $\sim 0°$), significantly different from the direction of the major axis (P.A. $= -30°$) of the central nebula.

Upon a closer inspection of the channel maps, however, we notice a systematic positional change of the fast components with V_{LSR}. Figure 6 shows the fast components extracted from channel maps of HCO^+ and HCN overlaid with H_2 emission. Figure 7 is a sketch of our interpretation of Figure 6 described below.

In Figure 2 for HCO^+ (3–2), the fast red components show a noticeable positional shift from (0″, −4″) in the most redshifted channel ($V_{LSR} = 46.9$ km s^{-1}) to (−1″, −7″) in the less redshifted channel (44.2 km s^{-1}). The southern, less redshifted

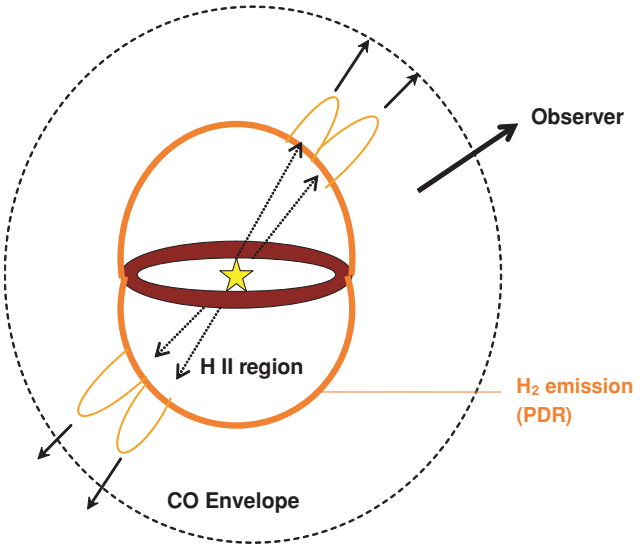

Figure 7. Geometrical model for NGC 7027. The figure schematically shows the relations and orientations among the torus, the H_2 emitting layer, and the outflows.

component is recognizable at (−1″, −7″) at an even slower velocity (41.4 km s^{-1}). The positional difference is clear in Figure 6 for the fast redshifted emission of HCO$^+$. A similar positional shift is found in fast red emission of HCN from the 47.8 km s^{-1} channel to the 42.3 km s^{-1} channel in Figure 5. Figure 6 demonstrates the positional shift.

Likewise, the fast blue components of HCO$^+$ show a positional shift from (−2″, +4″) in the most blueshifted channel (3.2 km s^{-1}) to (+1″, +5″) in the less blueshifted channel (8.7 km s^{-1}; Figure 2). The shift is clearly seen in the overlay of the contours for the two different velocities in Figure 6. The positional shift is less obvious in the HCN channel maps for the fast blue components (Figure 5). The most blueshifted channel (3.8 km s^{-1}) of HCN emission shows a compact component at (−2″, +3″). This component extends to (0″, +7″) in the less blueshifted channel (6.6 km s^{-1}) while the peak position stays at the same position (−2″, +3″). The extension of contours toward the north is explained as a blend of two components at different positions. The extended part of the HCN emission in the 6.6 km s^{-1} channel is explained as the result of the above-mentioned positional shift. The location of the extended part of the HCN emission is consistent with that of the blue HCO+ emission (Figure 6).

The positional shifts of similar trends (similar direction, similar amount of displacement, with similar degree of velocity change) in two molecules point to a common phenomenon, not a random noise. These positional shifts also seem abrupt with the change of velocity. These considerations lead us to an interpretation that the fast components actually consist of two kinematically distinct components. Below, we discuss this idea.

Even though the fast components have been observed for a long time, their accurate locations had not been determined at a 1″ accuracy until recent H_2 observations. In comparison with CO and H_2 emissions, the HCO$^+$ and HCN emissions in the present observations are fragmented or patchy, and strong line emissions of HCO$^+$ and HCN tend to originate from the prominent peaks of H_2 emission. The velocities and locations in the channel maps of the fast components most likely are manifestations of two bipolar outflows.

As shown in Figure 6, one of the identified outflows appears at P.A. = −10° and with velocity shifts of ±21 km s^{-1} (with respect to the systemic velocity). The projected location of the flow is close to the center, so that it appears overlapped with the H II region on the plane of sky. Hereafter, this outflow is referred to as the H-1 outflow with P.A. = −10°. The present identification of the H-1 outflow is consistent with early observations in HCO$^+$ (1–0) by Likkel (1992) and CO (3–2) by Jaminet et al. (1991). As will be discussed below, the H-1 outflow corresponds to the L-2 flow by Latter et al. (2000) (= the C-3 flow by Cox et al. 2002).

The other bipolar outflow has P.A. = +9° and velocity shifts of ±18 km s^{-1} (with respect to the systemic velocity). The blueshifted and redshifted lobes of this second outflow are located farther to the north and south than the first outflow (Figure 6). Also, the lobes of the second flow show good positional correlations with the bulging structure (to the north and south) in the H_2 image (Figure 6). This second flow in the present work will be referred to as the H-2 flow with P.A. = +9°. As will be discussed below, the H-2 flow corresponds to the C-2 flow by Cox et al. (2002).

The possible two outflows H-1 and H-2 appear in HCN maps in a pattern similar to those in HCO$^+$ maps, except the possible two outflows are not clearly separated in the present HCN observations. The two outflows occur at velocity shifts of ±21 km s^{-1} (P.A. = −12°, the H-1 flow) and ±18 km s^{-1} (P.A. = +2°, the H-2 flow).

The apparent axes of the H-1 outflows of both HCO$^+$ and HCN do not pass through the central star. They seem to correspond to the L-2 outflow in H_2 described as an off-axis flow by Latter et al. (2000). The H-1 outflow coincides in location with the C-3 outflow by Cox et al. (2002).

The flow axes of these fast components have position angles significantly different from the position angle of the overall major axis of the NGC 7027 envelope. These multiple outflows are probably manifestations of the possible BRETs in NGC 7027.

In addition to the outflows identified from the fast components, there are hints of an additional outflow. These hints of an outflow are identified based on comparisons with H_2 images and on a point-symmetric nature in position and velocity of some emission features of HCO$^+$. One possible pair is located at (a) (+10″, −7″) (in the SE side, 12″ from the center) with V_{LSR} = 19.6 km s^{-1} and at (b) (−6″, +6″) (in the NW side, 9″ from the center) with V_{LSR} = 30.5–33.3 km s^{-1}. These V_{LSR} values correspond to velocity shifts of ±6 km s^{-1} from the systemic velocity. The two emission spots are aligned along a P.A. = −54° line. The line coincides with that of the L-1 outflow in H_2 by Latter et al. (2000) (= the C-1 outflow by Cox et al. 2002). The positions of these HCO$^+$ emission features coincide with the extruding features toward NW in the H_2 images. The sense of velocity shifts of HCO$^+$ indicates that (1) the NW side is receding and (2) the SE side is approaching. However, the sense of velocity shifts of the HCO$^+$ emissions are opposite to those of the Brγ line (Cox et al. 2002): the NW side is blueshifted in the Brγ emission and the SE side is redshifted.

4. DISCUSSION

The fast components have been detected in HCO$^+$ (3–2, 4–3), HCN (3–2, 4–3), CN (N = 3–2, J = 7/2–5/2), and C_2H (N = 4–3, J = 9/2–7/2 and 3–2, 7/2–5/2; Hasegawa & Kwok 2001), as well as in the several rotational transitions of CO. There have been only a few observations that enable us to constrain the locations and sizes of the fast components. In early

interferometry work in CO (1–0), only the fastest components with velocity shifts larger than the bulk expansion velocity have been detected (Masson et al. 1985; Jaminet et al. 1991; Bieging et al. 1991). The locations of the fast CO components were better constrained later by Graham et al. (1993) and Fong et al. (2006; as a single bipolar flow with ∼6″ resolutions). The fast HCO^+ (3–2) and HCN (3–2) components (the H-1 and H-2 flows combined) with velocity shifts larger than 15 km s^{-1} are located in the same region as the fast CO components identified by Graham et al. (1993) and Fong et al. (2006). The coincidences in position and velocity strongly indicate that the HCO^+ and HCN fast components (H-1 and H-2 flows combined) in the present work and the CO fast components in the previous work reside in the same volume and are caused by a common mechanism. The CO, HCO^+, and HCN fast components are all likely driven by the same, unseen outflow phenomenon. The underlying outflow(s) must be point symmetric and must be well collimated, because only small (point-like) parts of the thick molecular envelope surrounding the central nebula show relatively fast and point-symmetric movements. The underlying collimated outflows possibly (1) originate from the central star (or very close to it), (2) have penetrated the H II region, and (3) impinge and bore into the molecular envelope.

As discussed in Section 3.4, the fast components of HCO^+ and HCN actually consist of two distinct flows (H-1 and H-2). The overlay of the fast HCO^+ components with the *HST* image at 2.12 μm in Figure 6 shows that the HCO^+ outflow H-1 coincides in position with the off-axis outflow (L-2) in the H_2 image (Latter et al. 2000). Similar to H_2, the axis of the outflow H-1 (seen in HCO^+ (3–2) and HCN (3–2)) has an offset of about 1″ from the center. The extruding H_2 feature in Figure 2(a) in Latter et al. (2000) has an appearance of coming out of an average H_2 surface at (0″, +5″).

The velocity shifts of ±21 km s^{-1} in the H-1 outflow include projection effects (see Figure 7). If the inclination of the flow axis from the line of sight is about 45°, the actual outward velocities are about ±30 km s^{-1}. This value is larger than the expansion velocity of 16.7 km s^{-1} of the equatorial ring and the bulk molecular envelope. The velocity shifts on small scales are another indication that some form of force is exerted over a very small solid angle. Again, an unseen collimated energetic outflow is a reasonable explanation.

The northern part (blueshifted) of the axis of the H-1 flow is probably tilted toward the observer from the plane of sky by 40°–60°. The entry point of the approaching (blueshifted) part of the putative jet (that causes the H-1 outflow) into the molecular envelope is seen by the observer as projected onto the central nebula. The entry point (of the blueshifted unseen jet causing H-1) into the molecular envelope corresponds to an exit point (of the flow) from the central nebula. The impinging jet causes a dent (or even bores a deep hole) in the thick molecular envelope. The inner surface of the dented part of the molecular envelope is exposed to the UV radiation from the central star, which results in H_2 emission. The resultant image has an appearance of an extruding surface. The fast emissions of HCO^+ (3–2) designated as outflows H-1 and H-2 most likely originate near the affected volume of the molecular envelope. The affected volume likely corresponds to a thin layer between the molecular envelope and the H II or outflowing gas, and are exposed to the UV radiation as well as are affected by a likely shock. The localized strong HCO^+ and HCN emissions can be a result of (1) localized favorable excitation conditions (a high density or a high temperature arising from a shock or a UV heating) or (2) a chemical enhancement (by a PDR chemistry or a shock chemistry). All these factors may be contributing in combination. However, a shock chemistry is unlikely to cause an abundance enhancement of HCO^+. In AFGL 2688, a PPN without an ionized region, shocked molecular regions have been detected in H_2 lines (Cox et al. 1997), but HCO^+ has not been detected (Bachiller et al. 1997). Bachiller et al. (1997) demonstrate that the presence of HCO^+ is closely related to the presence of ionizing photons in evolved stars and PNe. Hence, in the HCO^+ emission spots detected in the present work, a shock would not be a dominant process to enhance the abundance of HCO^+.

The present work demonstrates that the outflow-affected parts of molecular envelope contain heavy molecules other than CO and H_2. The presence of HCO^+ is in particular significant in that HCO^+ is newly formed in an evolved star after it starts ionizing the ejected molecular envelope (Bachiller et al. 1997). The HCO^+ emission is detected in regions surrounding the central H II region in NGC 7027. The presence of HCO^+ is explained as a result of photochemistry in a photon-dominated region. An emission enhancement would readily occur if the gas temperature or the density (electron in particular) is enhanced (Hasegawa & Kwok 2001). From the present observations, however, it is difficult to determine whether the enhanced HCO^+ emission at the likely interface regions reflect a chemical enhancement or an excitation enhancement.

Latter et al. (2000) and Cox et al. (2002) suggest another collimated outflow with P.A. $\sim -60°$. The present HCO^+ and HCN observation do not show any fast emission feature located at the extruding (or almost blown out) structure seen in the H_2 image. Instead, we find possible slow emissions at the same position and same position angle but with opposite sense of velocity shifts. If the possible multiple collimated outflows are not simultaneous but time-sequential, this working interface along P.A. $= -60°$ may no longer be active or molecules there may have been evacuated or destroyed. The evacuation scenario seems more likely. Fong et al. (2006) find regions devoid of CO along the P.A. $= -60°$ direction. Cox et al. (2002) find both X-ray emission (Kastner et al. 2001) and high-velocity Brγ emission along the P.A. $= -60°$ direction.

5. SUMMARY

We observed the young PN NGC 7027 in HCO^+ (3–2) and HCN (3–2) with the SMA with ∼3″ resolution. The observations show prominent HCO^+ emission from the equatorial torus and the geometrically thin, curved layer surrounding the central H II region. The HCO^+ emitting regions likely correspond to a chemically active PDR. In addition, we constrained the locations and extents of the fast emissions of HCO^+ and HCN with the ∼3″ accuracy. The fast components of HCO^+ and HCN emissions coincide in velocity and location with the previously known fast CO components (Graham et al. 1993; Fong et al. 2006) detected at ∼6″ resolutions.

The HCO^+ and HCN fast components likely consist of two kinematically different bipolar flows, corresponding to two extruding features identified by Latter et al. (2000) and Cox et al. (2002) in H_2 observations. The two bipolar flows detected in HCO^+ and HCN are likely caused by acceleration of molecular envelope by unseen collimated jets impinging into the molecular envelope of NGC 7027. The axes of the HCO^+ and HCN flows (and the underlying jets) are not aligned with the overall symmetric axis common to the central H II region and the

hourglass morphology of the H_2 emission. These are indications of multiple jets or a single jet that changes its direction.

We thank the SMA staff for their efforts in running and maintaining the array. This work was partly supported by the NSC grant 96-2112-M-001-018-MY3 to T.I.H. S.K. acknowledges support from the Research Grants Council of the Hong Kong Special Administrative Region, China (Project No. HKU 7031/10P).

REFERENCES

Atherton, P. D., Hicks, T. R., Reay, N. K., Robinson, G. J., Worswick, S. P., & Phillips, J. P. 1979, ApJ, 232, 786
Bachiller, R., Forveille, T., Huggins, P. J., & Cox, P. 1997, A&A, 324, 1123
Bains, I., Bryce, M., Mellema, G., Redman, M. P., & Thomasson, P. 2003, MNRAS, 340, 381
Balick, B. 1996, Am. Sci., 84, 342
Basart, J. P., & Daub, C. T. 1987, ApJ, 317, 412
Bieging, J. H., Wilner, D., & Thronson, H. A., Jr. 1991, ApJ, 379, 271
Bryce, M., Balick, B., & Meaburn, J. 1994, MNRAS, 266, 721
Cox, P., Huggins, P. J., Maillard, J.-P., Habart, E., Morisset, C., Bachiller, R., & Forveille, T. 2002, A&A, 384, 603
Cox, P., et al. 1997, A&A, 321, 907
Deguchi, S., Izumiura, H., Nguyen-Q-Rieu, Shibata, K. M., Ukita, N., & Yamamura, I. 1992, ApJ, 392, 597
Fong, D., Meixner, M., Sutton, E. C., Zalucha, A., & Welch, W. J. 2006, ApJ, 652, 1626
Graham, J. R., Serabyn, E., Herbst, T. M., Matthews, K., Nuegebauer, G., Soifer, B. T., Wilson, T. D., & Beckwith, S. 1993, AJ, 105, 250
Hasegawa, T. I., & Kwok, S. 2001, ApJ, 562, 824
Ho, P. T. P., Moran, J. M., & Lo, K. Y. 2004, ApJ, 616, L1
Hoare, M. G., Roche, P. F., & Clegg, R. E. S. 1992, MNRAS, 258, 257
Jaminet, P. A., Danchi, W. C., Sutton, E. C., Russell, A. P. G., Sandell, G., Bieging, J. H., & Wilner, D. 1991, ApJ, 380, 461
Kastner, J. H., Vrtilek, S. D., & Soker, N. 2001, ApJ, 550, L189
Knapp, G. R., Sandell, G., & Robson, E. I. 1993, ApJS, 88, 173
Latter, W. B., Dayal, A., Bieging, J. H., Meakin, C., Hora, J. L., Kelly, D. M., & Tielens, A. G. G. M. 2000, ApJ, 539, 783
Likkel, L. 1992, ApJ, 397, L115
López, J. A., Vázquez, R., & Rodríguez, L. F. 1995, ApJ, 455, L63
Masson, C. R. 1986, ApJ, 302, L27
Masson, C. R. 1989, ApJ, 336, 294
Masson, C. R., et al. 1985, ApJ, 292, 464
Phillips, J. P., Mampaso, A., Williams, P. G., & Ukita, N. 1991, A&A, 247, 148
Roelfsema, P. R., Goss, W. M., Pottasch, S. R., & Zijlstra, A. 1991, A&A, 251, 611
Sahai, R. 2000, in ASP Conf. Ser. 199, Asymmetric Planetary Nebulae II, ed. J. H. Kastner, N. Soker, & S. Rappaport (San Francisco, CA: ASP), 209
Zhang, C. Y., & Kwok, S. 1998, ApJS, 117, 341